Materials Today Physics 15 (2020) 100259

Contents lists available at ScienceDirect

Materials Today Physics

journal homepage: https://www.journals.elsevier.com/materials-today-physics

# Temperature dependent optical characteristics of all-inorganic $CsPbBr_3$ nanocrystals film

X.Y. Zhang [a], G.T. Pang [a], G.C. Xing [b, *], R. Chen [a, c, *]

[a] Department of Electrical and Electronic Engineering, Southern University of Science and Technology, Shenzhen, 518055, China
[b] The Institute of Applied Physics and Materials Engineering, University of Macau, Avenida da Universidade, Taipa, Macau, China
[c] Key Laboratory of Energy Conversion and Storage Technologies (Southern University of Science and Technology), Ministry of Education, Shenzhen, 518055, China

ARTICLE INFO

*Article history:*
Received 14 July 2020
Received in revised form
1 August 2020
Accepted 1 August 2020
Available online 8 August 2020

*Keywords:*
Perovskite
Laser spectroscopy
Optical property
Surface state

ABSTRACT

As one of the most promising optoelectronic materials in recent years, colloidal all-inorganic lead halide perovskite nanocrystals (NCs) have become a research focus. An in-depth understanding of electron behavior in the material is essential for advanced device application. Here, temperature-dependent photoluminescence (PL) spectroscopy is employed to study the optical properties of $CsPbBr_3$ NCs film. It is found that the PL intensity decreased with temperature below 200 K, while reverse trend has been observed with temperature above 200 K. The mechanism of the PL unusual quenching phenomenon is attributed to surface states of NCs, which leads to non-radiative recombination of electrons at low temperatures. Above the critical temperature, electrons will escape from the defect level and participate in radiative recombination, which give rise to the enhanced emission. The model is further verified by comparison with nanoplatelets, surface passivation, as well as temperature-dependent PL decay experiments.



## 1. Introduction

As an emerging material, perovskite has shown an amazing development speed in just the past decade. The efficiency of perovskite solar cells has jumped rapidly from 3.8% [1] to 25.2% [2], which is now comparable to polysilicon solar cells [3]. At the same time, perovskite materials also possess broad prospects in optoelectronic applications, such as bioimaging [4], photodetector [5], and light-emitting devices (LEDs) [6,7], lasing [8], thermoelectric field [9], etc. Among the major classes of perovskite structures, organic-inorganic hybrid perovskite solar cells have achieved recorded performance because of their unique properties [10–12]. Unfortunately, their poor environmental stability prevents the practical applications [13]. Compared to the hybrid perovskites, the all-inorganic lead-halide perovskite has attracted more intensive research attention because of its better stability [14], which is considered to be more suitable for industrialization. However, the inorganic lead-halide perovskite bulk crystals manifest very poor optical properties due to the small exciton binding energy. When the size of crystals reduces to the nanometer level, the situation becomes completely different. The reduced dimensionality results in the increase of material's exciton binding energy [15,16]. Meanwhile, the electron-phonon coupling in perovskite is important for photovoltaic applications. The strong inhomogeneous emission line broadening [17] inherited from bulk samples obscures the spectral features of phonons, which hinders the basic research as well as the application of these materials. Thus, the inorganic perovskite nanocrystals (NCs) have been considered as a particularly attractive material for next-generation lighting and display technology. Compared with the traditional low-dimensional semiconductors such as CdSe [18], $CsPbX_3$ (X = Cl, Br, I) NCs are recognized as a better candidate for light sources in the blue, green, and red spectral region. Lots of researches on the carrier kinetics of these perovskites have been carried out [19–21]. However, the understanding of their optical properties, especially the photoluminescence (PL) evolution with temperature is far from enough. Such information is very important for the application of the materials operated at different temperatures. Therefore, it is necessary to study the photophysical properties of these $CsPbX_3$

* Corresponding authors.
*E-mail addresses:* gcxing@um.edu.mo (G.C. Xing), chenr@sustech.edu.cn (R. Chen).

https://doi.org/10.1016/j.mtphys.2020.100259
2542-5293/

NCs to fully realize their potential, and further provide new breakthroughs for basic research and commercial applications.

It is widely accepted that the temperature-dependent PL spectroscopy is an effective technique to study the nonradiative relaxation processes and exciton-phonon coupling in semiconductors [22–24]. Generally speaking, the integrated PL intensities of traditional semiconductors decrease with increasing temperature, which is known as the thermal quenching of PL. The thermal quenching behavior is usually related to carrier trapping by large amount of non-radiative states/traps or thermal dissociation of excitons assisted by the scattering with multiple longitudinal optical (LO) phonons. Many reports on the temperature-dependent PL spectra of $CsPbBr_3$ NCs have shown that the thermal quenching exists at temperature up to 200 K [25–27]. However, little attention has been paid to the abnormal phenomenon that occurs above 200 K, that is, the PL intensity increase with temperature. Although it could be found in some reports [28,29], the physical mechanism of this phenomenon has not been thoroughly explored and explained.

In this study, in order to investigate the origin of the unusual quenching of PL, colloidal $CsPbBr_3$ NCs film was prepared. By comparing the temperature-dependent PL spectra of all-inorganic lead-halide perovskite materials under different excitation densities and surface passivation experiment, it is noted that the unusual quenching behavior of PL is related to the defects on the surface of this material. In addition, the corresponding investigations carried out on $CsPbBr_3$ nanoplatelets (NPLs) with more surface defects have also further confirmed our conclusions. Our experimental results provide new insight into the photophysical mechanism of excitons in all-inorganic perovskite nanocrystals, which helps to clarify their potential for high-performance optoelectronic devices.

## 2. Materials and methods

### 2.1. Sample preparation

Colloidal $CsPbBr_3$ NCs were synthesized by a hot-injection approach. First, $PbBr_2$ and octadecene were loaded into a 50 mL 3-neck flask, degassed at 120 °C for 30 min. Oleylamine and oleic acid were injected at 120 °C under $N_2$. After complete solubilisation of a $PbBr_2$ salt, the temperature was heated to 160 °C and Cs-oleate solution obtained by dissolving $CsCO_3$ in octadecene and oleic acid at 150 °C was quickly injected. After 5 s, the reaction mixture was cooled by the ice-water bath. The films for temperature-dependent PL measurements and passivation experiments were fabricated via dropping colloidal NCs solution on quartz substrates. For comparison, polydimethylsiloxane (PDMS) was used to passivate the $CsPbBr_3$ film.

### 2.2. Morphology characterization

Transmission electron microscope (TEM) samples were prepared through dropping colloidal NCs solution with relatively dilute concentration on carbon-coated 200 mesh copper TEM grids. And the conventional TEM image was acquired by a Talos F200X microscope equipped with a thermionic gun with an acceleration voltage of 200 kV. The current of the 1 nm electron beam at this voltage is 1.5 nA, and the resolution is 0.12 nm.

### 2.3. Optical measurement

Measurements of the linear absorption and absolute photoluminescence quantum yields (PLQY) were performed by a UV–vis–NIR spectrophotometer (Lambda 950, PerkinElmer, Inc.) and a spectrometer (Zolix, SENS-9000), respectively. $CsPbBr_3$ NCs film was placed inside a closed-cycle helium cryostat with quartz windows for PL measurements. The PL spectra were recorded using a charge coupled device (CCD). A 325 nm continuous wave (CW) He–Cd gas laser was used as the excitation source. The temperature during the PL measurement is well-controlled from 50 to 295 K. Time-resolved photoluminescence (TRPL) experiments were carried out at room temperature. The excitation source was a pulsed ultraviolet picosecond diode laser operating at 375 nm. The pulse width and repetition rate of the laser were 40 ps and 20 MHz, respectively. The signal was dispersed by a 320 mm monochromator (iHR320 from Horiba, Ltd.) combined with suitable filters and detected based on the time-correlated single photon counting (TCSPC) technique.

## 3. Results and discussion

The TEM image of the perovskite NCs is shown in Fig. 1(a), which indicates that the NCs possess nearly cubic shape with size about 15 nm. The excellent dispersibility can be attributed to the ligands on the surface of the $CsPbBr_3$ NCs. Fig. 1(b) shows the normalized absorption and PL spectra of the perovskite $CsPbBr_3$ NCs film. It can be observed that the absorption band was very broad at room temperature, which should be induced by the inhomogeneous size distribution [30]. Strong PL emission can be observed at 519 nm with a full width at half maximum (FWHM) of 17.3 nm. The emission peak is slightly red-shifted to the absorption peak. The PL spectral properties of the NCs are similar to those reported recently in literatures [31,32]. Furthermore, the Stokes shift is around 12 nm, which indicates that the PL emission of NCs may originate from the radiative recombination of free excitons or bound excitons at room temperature [33,34]. The emission decay is illustrated in the inset of Fig. 1(b), and the average PL lifetime of all-inorganic perovskite $CsPbBr_3$ NCs is 4.02 ns. The value is orders of magnitude faster than other optoelectronic materials with a typical decay time longer than 100 ns, such as CdSe [35]. This implies that perovskite NCs are more suitable for application in LEDs, lasers, photodetectors and other optoelectronic devices.

Fig. 2(a) shows the 2D pseudo-color plot of the temperature-dependent PL spectrum. Obviously, the PL peaks show the tendency of the blueshift with temperature increases from 50 to 295 K with a total shift of 5.3 nm, while the FWHM significantly increases within the same temperature range. Similar phenomenon has been reported in many literatures for Pb-based perovskites and other Pb-based semiconductors, such as PbSe [36,37]. It is worth noting that the PL intensities of $CsPbBr_3$ NCs film exhibit a decrease from 50 to 200 K. While for the temperature range between 200 and 295 K, the PL intensity increases with temperature, which is very different from the previous literatures [38,39].

A detailed analysis of the PL spectra within the two temperature ranges was discussed in order to explore the unusual characteristics. The photon energy, FWHM and the integrated PL intensity of $CsPbBr_3$ NCs film at temperature ranging from 50 to 295 K are shown in Fig. 2(b)–(d). Under constant pressure, the temperature-dependence of the bandgap can be generally described by the following expression under a quasi-harmonic approximation [40],

$$\frac{\partial E_g}{\partial T} = \frac{\partial E_g}{\partial V}\frac{\partial V}{\partial T} + \sum_{j,\vec{q}}\left(\frac{\partial E_g}{\partial n_{j,\vec{q}}}\right)\left(n_{j,\vec{q}} + \frac{1}{2}\right) \quad (1)$$

where $n_{j,\vec{q}}$ is the number of phonons at $j$ branch with wave vector of $\vec{q}$, and it follows the Bose-Einstein distribution:

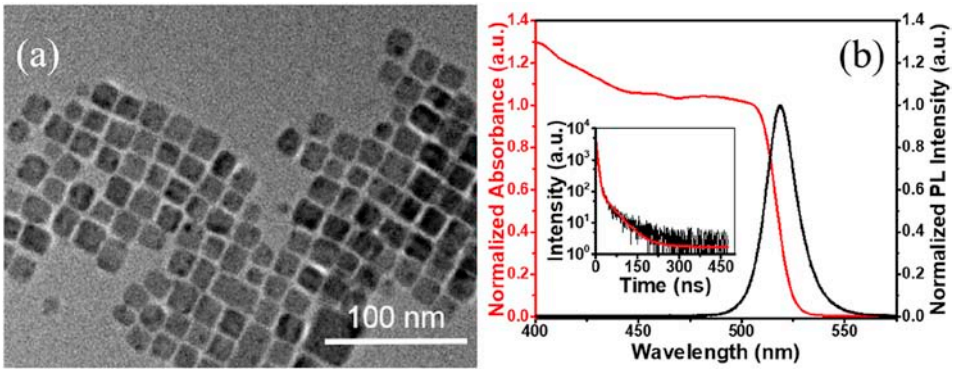


**Fig. 1.** (a) The TEM image of perovskite $CsPbBr_3$ NCs film. (b) Absorption (red line) and photoluminescence (black line) spectra at room temperature. The inset is the TRPL of $CsPbBr_3$ NCs film at room temperature. (For interpretation of the references to color in this figure legend, the reader is referred to the Web version of this article.)

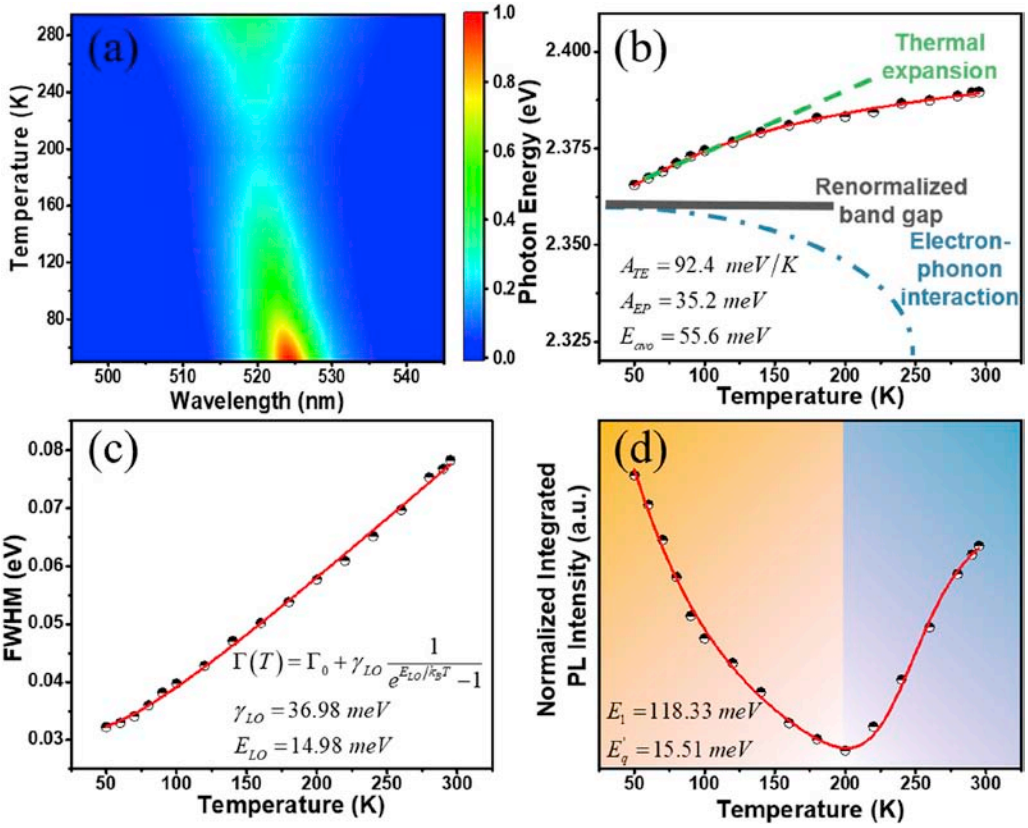


**Fig. 2.** (a) The normalized PL spectra of a 2D pseudo-color plot of the NCs film at temperature ranging from 50 to 295 K. (b) The photon energy as a function of temperature extracted out from (a); black dots: experimental data and the red line: the fitting curve. The green dashed and the bule dashed-dotted lines show the individual contributions of TE and EP interaction. (c) The FWHM as a function of temperature; black dots: experimental data and red line: the fitting curve. (d) The integrated PL intensity as a function of temperature; black dots: experimental data and red line: the fitting curve.

$$n_{j,\vec{q}} = \frac{1}{\exp(\hbar\omega_{j,\vec{q}}/k_B T - 1)} \tag{2}$$

where $\omega_{j,\vec{q}}$ is the angular frequency of the phonon mode. The first part of Equation (1) on the right describes the contribution of the thermal expansion (TE) of the lattice. The coefficient $\partial E_g/\partial V$ depends weakly on temperature and thus can be regarded as a constant. Its value can be either positive or negative, depending on the specifics of the bonding parameters as well as the detailed structure of the bandgap. The band structure calculation of $CsPbBr_3$ displays that the valence band maximum is determined by the hybridization between the *p* orbit of Br and *s* orbit of Pb [32]. With the increase of temperature, TE of the lattice will decrease the interaction between these two orbits, resulting in a decrease of the valance bandwidth and an increase of the bandgap. So here, the value of $\partial E_g/\partial V$ is positive. The second part of Equation (1) is attributed to the exciton-phonon (EP) interaction. Combined with TE, Equation (1) can be simplified to the following expression by assuming a linear relationship between lattice constant and temperature [41],

$$E(T) = E_0 + A_{TE}T + A_{EP}\left[\frac{2}{\exp(E_{avo}/k_BT) - 1} + 1\right] \quad (3)$$

where $E_0$ is the unrenormalized bandgap, $A_{TE}$ and $A_{EP}$ are the weight of the TE and EP interaction, respectively, and $E_{avo}$ is the average optical phonon energy. Due to the quantum factor in the phonon distribution function, there is an energy correction of the bandgap even at zero temperature, namely $E_g(T = 0) = E_0 + A_{EP}$.

Fig. 2(b) shows the fitted results of photon energy and the parameters extracted are $E_0$ = 2.43 eV, $A_{TE}$ = 92.4 μeV $K^{-1}$, $A_{EP}$ = 35.2 meV and $E_{avo}$ = 55.6 meV. To highlight the contribution of the TE and the EP interaction, both are added to the renormalized bandgap (Eg (T = 0)). It clearly shows that the linear-increased PL peak can be derived from the domination of TE (the green dashed line) at low temperature, while EP interaction (blue dashed-dotted line) is negligible due to the unsubstantially populated optical phonon modes. However, for higher temperatures, the optical phonon modes are appreciably populated, which leads to a significant negative contribution. This is why the trend of the increase of photon energy is slowing down.

As shown in Fig. 2(c), the FWHM broadens monotonously with increasing temperature. The analysis of temperature-dependent emission broadening has long been used to evaluate the mechanism of exciton-phonon coupling in a large number of inorganic semiconductors. The emission broadening can be expressed as [42],

$$\Gamma(T) = \Gamma_0 + \gamma_{LO}\frac{1}{e^{E_{LO}/k_BT} - 1} \quad (4)$$

where $\Gamma_0$ is the term of a temperature-independent inhomogeneous broadening, which results from the disorder and imperfection scattering. The second term is the homogeneous broadening, which arises from LO phonon-carrier scattering. $\gamma_{LO}$ and $E_{LO}$ are EP coupling strength and the LO phonon energy, respectively. The fitting result of the temperature-dependent PL line-width with temperature using Equation (4) was plotted in Fig. 2(c), yielding the coupling strength $\gamma_{LO}$ = 37.0 meV and an average phonon energy of $E_{LO}$ = 14.9 meV.

Fig. 2(d) shows the integrated PL intensity of $CsPbBr_3$ NCs film. The emission intensity from most of semiconductors is normally observed to decrease monotonically with temperature, which is called PL thermal quenching. The basic mechanism of PL quenching is attributed to the increase of the nonradiative recombination probability of electrons and holes with increasing temperature. However, for $CsPbBr_3$ NCs film, it can be seen that at higher temperature range (200–295 K), the PL intensity increases with temperature. The integrated PL intensity of thermal quenching can be fitted by the well-known expression [43,44],

$$I(T) = \frac{I_0}{1 + CT\exp(-E_a/k_BT)} \quad (5)$$

where $I_0$ is the PL intensity at low-temperature limit, $E_a$ is activation energy, $k_B$ is the Boltzmann constant, and $C$ is constant. However, for $CsPbBr_3$ NCs film, the PL intensity shows an unusual quenching of PL at higher temperature, which has been observed in many semiconductors and may be attributed to either delocalization of carriers [45,46] or quenching of the nonradiative defects [47]. It can be described by a modified expression [48,49],

$$I(T) = I(0)\frac{1 + \sum_{q=1}^{w} D_q \exp\left(-E_q'/k_BT\right)}{1 + \sum_{j=1}^{m} C_jT\exp(-E_j/k_BT)} \quad (6)$$

where $E_q'$ describes the activation energies for processes that increases the PL intensity with increasing temperature. The fitting result shown in Fig. 2(d) gives $E_1$ = 118.3 meV for $CsPbBr_3$ NCs film, which is well consistent with the exciton binding energy, and $E_q'$ = 15.5 meV.

In order to explore the unusual quenching phenomenon, temperature-dependent PL measurements under different excitation densities were conducted. The integrated PL intensity extracted from the temperature-dependent PL spectrum under three different excitation powers, namely 0.05, 0.50 and 5.00 mW, respectively, can be found in the Supporting Information (Fig. S2). Detail experimental data can be found in Fig. S3. In Fig. 3, the PL intensity at 50 K was normalized for easier comparison. It is noted that there is a big difference of integrated PL intensity with temperature under different excitation conditions. Under low excitation power (0.05 mW), the integrated PL intensity decreases all the way with temperature. For moderate excitation power (0.50 mW), the integrated PL intensity decreases first below 200 K and then rises after the temperature above 200 K (region II). For high excitation power (5.00 mW), the integrated PL intensity increases within a very narrow temperature range from 180 to 200 K (region I), and then decreasing with further increase of temperature.

The schematic diagram of defects level near the conduction band (CB) is proposed to explain the differences, as shown in Fig. 4. It is known that the PL intensity depends on both the radiative recombination efficiency and the relaxation of the hot carriers. In that sense, the whole electronic structure may influent the PL signature. For $CsPbBr_3$ nanocrystals, the phase transition occurs between 361 and 403 K [50]. There is no phase transition during the temperature-dependent measurement and the electronic structure of $CsPbbr_3$ NCs film remains the same. The defects level is about 15 meV lower than CB, which is almost the same as the average phonon energy ($E_{LO}$ = 14.9 meV) of $CsPbBr_3$ NCs, so that electrons can be more easily captured by defects by coupling with the phonon. With the increase of temperature, bound electrons will escape from the defect level and participate in radiative recombination, which give rise to the enhanced PL intensity. Beside thermal energy, collision between electrons under high excitation power is needed to be taken into consideration.

For low excitation power (0.05 mW), the laser thermal effect and collision between electrons are negligible. Due to the limited

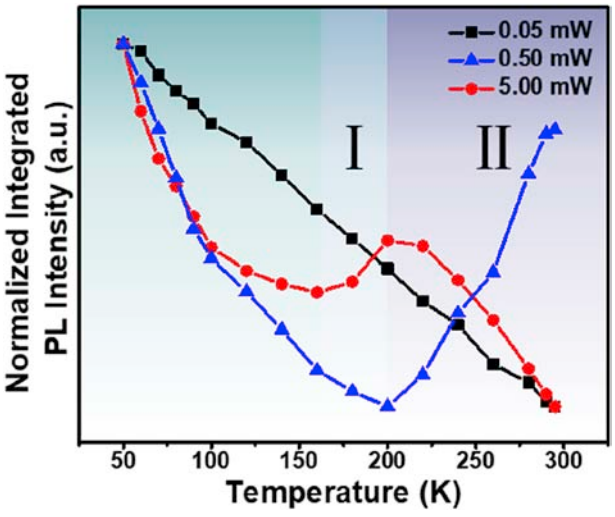


**Fig. 3.** The integrated PL intensity as a function of temperature under different power conditions.

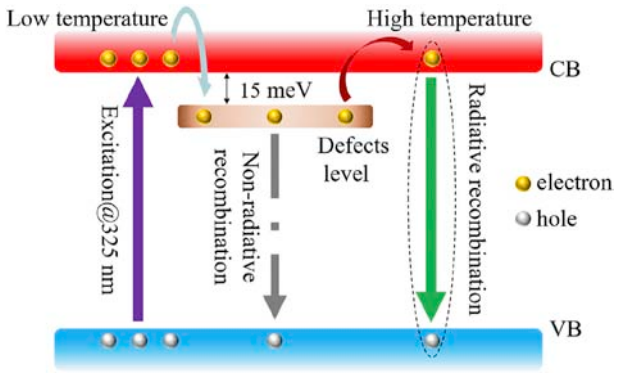


**Fig. 4.** Schematic model of unusual quenching in $CsPbBr_3$ NCs film.

number of electrons released from the defects and the existence of thermal quenching, there is no apparent increase of emission intensity at high temperature. Therefore, the integrated PL intensity decreases all the way. For moderate excitation power (0.50 mW), more electrons will release from the defect level under high temperature. Those electrons compete with thermal quenching and contribute to the emission, which leads to an increase in integrated PL intensity above 200 K. For high excitation power (5.00 mW), due to the high density of electrons generated and limited defect state density, the escaped electrons contribute relatively weak to the emission, which results in a small incensement compared to the moderate excitation. Moreover, laser thermal effect and collision between electrons will be more serious which lead to non-radiative recombination. This is why the integrated PL intensity decreases with further increase of temperature above 200 K as shown in Fig. 3.

In order to confirm the correctness of the proposed model, surface passivation experiment and the temperature-dependent PL characterization of the treated $CsPbBr_3$ NCs film was employed. The comparison of the temperature-dependent PL spectra of $CsPbBr_3$ NCs film before and after passivation is shown in Fig. 5(a), and the integrated PL intensity were normalized according to the data point of 50 K. It is obvious that the treated $CsPbBr_3$ NCs film showed the thermal quenching behavior. The integrated PL intensity of treated sample is basically higher than $CsPbBr_3$ NCs film because of the reduction of defects. Therefore, the trap state is considered to be the defects on the material's surface. In addition, we also performed passivation experiment and temperature-dependent PL spectra of quasi-2D $CsPbBr_3$ NPLs film, which possess more surface defects than NCs due to the larger surface-to-volume ratio [51]. The results were shown in Fig. 5(b), and it can be clearly seen that NPLs have a more pronounced unusual quenching with the change of temperature. At the same time, there is still a slight unusual quenching behavior of PL in the passivated NPLs film during the change of temperature, which further confirms the correctness of the model proposed.

Finally, to reconfirm the above model, temperature-dependent PL lifetime measurement has been performed. In general, the PL lifetimes for most of colloidal quantum dots such as CdSe and PbS, decrease with increasing temperature due to dominant emission from exciton recombination [52,53]. However, the lengthening of the average PL lifetimes has also been observed in the colloidal CdSe quantum dots recently, which was explained by introducing the charge carrier trapping at surface states or localized states as relaxation pathway and using a classical charge transfer theory [35,54]. It can be seen that the PL lifetime increases monotonically from low to high temperature and shows a maximum (4.02 ns) at ~300 K, as shown in Fig. 6, which implies the existence of surface states or localized states in the $CsPbBr_3$ NCs. The interaction of excitons with surface states under high temperature may results in an increase of PL lifetime of NCs.

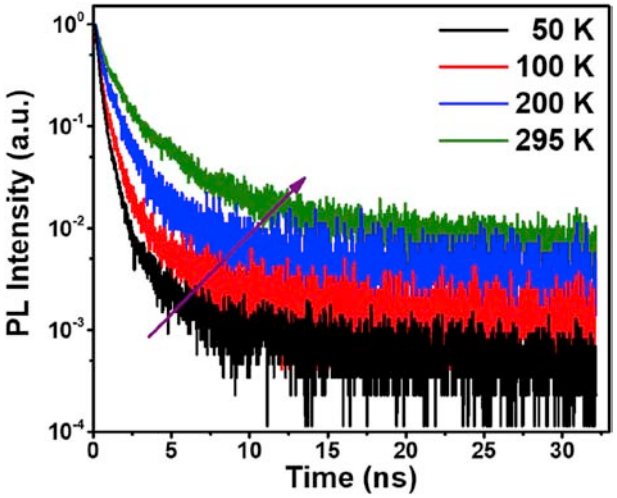


**Fig. 6.** Temperature-dependent PL decay excited by a 375 nm laser beam.

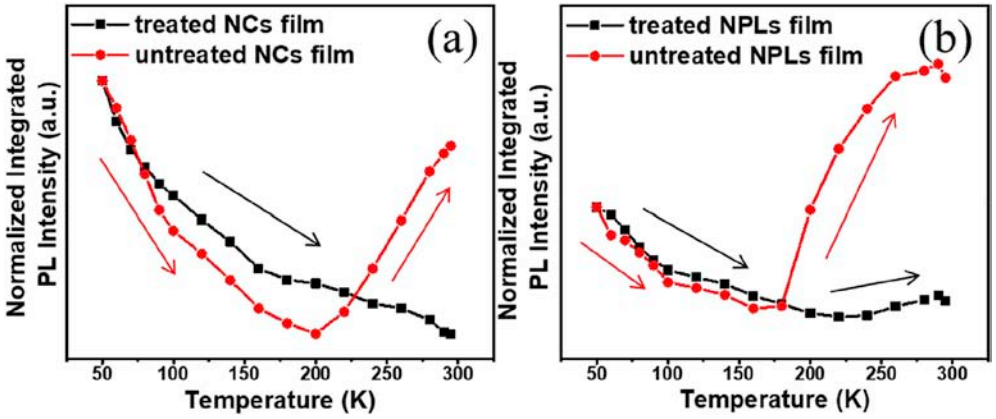


**Fig. 5.** (a) Comparison of the integrated PL intensity as a function of temperature of the treated NCs film and NCs film. (b) Comparison of the integrated PL intensity as a function of temperature of the treated NPLs film and NPLs film.

## 4. Conclusion

In summary, we studied the PL emission characteristics of all-inorganic perovskite $CsPbBr_3$ NCs using temperature-dependent PL spectroscopy. The photon energy and FWHM of $CsPbBr_3$ NCs film is basically consistent with those reported in other literatures, and PL emission is ascribed to the excitonic recombination. It is interesting to observe that the integrated PL intensity of $CsPbBr_3$ NCs film increases with temperature above 200 K. Through temperature-dependent PL measurement under different excitation powers and passivation experiments, the PL unusual quenching behavior is confirmed to be related to the surface defects of $CsPbBr_3$ NCs. At low temperature, surface defects will capture electrons which results in non-radiative recombination. With the increase of temperature, the trapped electrons will gain energy from collision or surrounding environment, then overcome the barrier and contribute to the emission, which leads to an increase of PL intensity. It is found that higher power will increase the release rate of electrons remarkably. Moreover, corresponding experiments were also performed on $CsPbBr_3$ NPLs film, and the results are in line with the model proposed. Finally, the temperature-dependent PL lifetime measurement further confirmed the existence of surface states in the samples. Our experimental results show that the reasonable use of surface states will boost the application of all-inorganic $CsPbBr_3$ NCs.

## Credit author statement

X.Y. Zhang, G.C. Xing and R. Chen conceived the experiment. G.T. Pang employed the transmission electron microscope. X.Y. Zhang carried out the temperature-dependent photoluminescence experiments and worked on the data analysis. All authors discussed the data and contributed to the manuscript.

## Declaration of Competing Interest

The authors declare that they have no known competing financial interests or personal relationships that could have appeared to influence the work reported in this paper.

## Acknowledgments

This work is supported by Shenzhen Science and Technology Innovation Commission (Projects Nos. JCYJ20180305180553701 and KQTD2015071710313656). G.X. acknowledges financial support from The Science and Technology Development Fund (File No. 091/2017/A2), a research grant (MYRG2018-00148-IAPME) from University of Macau, and the National Natural Science Foundation of China (91733302, 61605073, 61935017).

## Appendix A. Supplementary data

Supplementary data to this article can be found online at https://doi.org/10.1016/j.mtphys.2020.100259.

Acknowledgments.

## Data availability

The raw/processed data required to reproduce these findings cannot be shared at this time due to technical or time limitations.

## References

[1] A. Kojima, K. Teshima, Y. Shirai, T. Miyasaka, Organometal halide perovskites as visible-light sensitizers for photovoltaic cells, J. Am. Chem. Soc. 131 (2009) 6050–6051, https://doi.org/10.1021/ja809598r.
[2] F. Sahli, J. Werner, B. Kamino, M. Bräuninger, R. Monnard, B. Paviet-Salomon, L. Barraud, L. Ding, J. Leon, D. Sacchetto, Fully textured monolithic perovskite/silicon tandem solar cells with 25.2% power conversion efficiency, Nat. Mater. 17 (2018) 820–826, https://doi.org/10.1038/s41563-018-0115-4.
[3] M. Green, The path to 25% silicon solar cell efficiency: history of silicon cell evolution, Prog. Photovoltaics 17 (2009) 183–189, https://doi.org/10.1002/pip.892.
[4] K. Wang, H. Zhang, Z. Gu, All-inorganic perovskite nanocrystal materials: new generation of scintillators for high quality X-ray imaging, Sci. Bull. 64 (2019) 1205–1206, https://doi.org/10.1016/j.scib.2019.07.009.
[5] P. Ramasamy, D.-H. Lim, B. Kim, S.-H. Lee, M.-S. Lee, J.-S. Lee, All-inorganic cesium lead halide perovskite nanocrystals for photodetector applications, ChemComm 52 (2016) 2067–2070, https://doi.org/10.1039/C5CC08643D.
[6] G. Cheng, Y. Liu, T. Chen, W. Chen, Z. Fang, J. Zhang, L. Ding, X. Li, T. Shi, Z. Xiao, Efficient all-inorganic perovskite light-emitting diodes with improved operation stability, ACS Appl. Mater. Interfaces 12 (2020) 18084–18090, https://doi.org/10.1021/acsami.9b23170.
[7] D. Liang, Y. Peng, Y. Fu, M. Shearer, J. Zhang, J. Zhai, Y. Zhang, R. Hamers, T. Andrew, S. Jin, Color-pure violet-light-emitting diodes based on layered lead halide perovskite nanoplates, ACS Nano 10 (2016) 6897–6904, https://doi.org/10.1021/acsnano.6b02683.
[8] T. Masuda, Y. Zhang, C. Ding, F. Liu, K. Sasaki, Q. Shen, M. Endo, All-inorganic cesium lead halide perovskite nanocrystals for solar-pumped laser application, J. Appl. Phys. 127 (2020) 243104, https://doi.org/10.1063/5.0011945.
[9] X. Xiao, M. Widenmeyer, K. Mueller, M. Scavini, S. Checchia, C. Castellano, D. Ma, S. Yoon, W. Xie, U. Starke, K. Zakharchuk, A. Kovalevsky, A. Weidenkaff, A squeeze on the perovskite structure improves the thermoelectric performance of europium calcium titanates, Mater. Today Phys. 7 (2018) 96–105, https://doi.org/10.1016/j.mtphys.2018.11.009.
[10] C. Wehrenfennig, G.E. Eperon, M.B. Johnston, H.J. Snaith, L.M. Herz, High charge carrier mobilities and lifetimes in organolead trihalide perovskites, Adv. Mater. 26 (2014) 1584–1589, https://doi.org/10.1002/adma.201305172.
[11] S. D Stranks, G. E Eperon, G. Grancini, C. Menelaou, M. Alcocer, T. Leijtens, L. Herz, A. Petrozza, H. Snaith, Electron-hole diffusion lengths exceeding 1 micrometer in an organometal trihalide perovskite absorber, Science 342 (2013) 341–344, https://doi.org/10.1126/science.1243982.
[12] B. Chen, G. Pang, X. Lan, Z. He, R. Chen, Strong band filling induced significant excited state absorption in $MAPbI_3$ under high pump power, Mater. Today. Phys. 14 (2020) 100228, https://doi.org/10.1016/j.mtphys.2020.100228.
[13] B. Charles, J. Dillon, J. Weber, S. Islam, T. Weller, Understanding the stability of mixed A-cation lead iodide perovskites, J. Mater. Chem. 43 (2017) 22495–22499, https://doi.org/10.1039/C7TA08617B.
[14] B. Yang, J. Chen, F. Hong, X. Mao, K. Zheng, S. Yang, Y. Li, T. Pullerits, W. Deng, K. Han, Lead-free, air-stable all-inorganic cesium bismuth halide perovskite nanocrystals, Angew. Chem. Int. Ed. 56 (2017) 12471–12475, https://doi.org/10.1002/anie.201704739.
[15] L. Wirtz, A. Marini, A. Rubio, Excitons in boron nitride nanotubes: dimensionality effects, Phys. Rev. Lett. 96 (2006) 126104, https://doi.org/10.1103/PhysRevLett.96.126104.
[16] W. Ying, N. Herron, Dynamics of exciton formation and relaxation in GaAs quantum wells, Phys. Rev. B Condens. Matter 42 (1990) 7253–7255, https://doi.org/10.1103/PhysRevB.42.7434.
[17] H. Diab, G. Trippé-Allard, F. Lédée, K. Jemli, J. Even, Narrow linewidth excitonic emission in organic-inorganic lead iodide perovskite single crystals, J. Phys. Chem. Lett. 7 (2016) 5093–5100, https://doi.org/10.1021/acs.jpclett.6b02261.
[18] M. Choi, J. Yang, K. Kang, D. Kim, C. Choi, C. Park, S. Kim, S. Chae, T.-H. Kim, J.H. Kim, Wearable red–green–blue quantum dot light–emitting diode array using high–resolution intaglio transfer printing, Nat. Commun. 6 (2015), https://doi.org/10.1038/ncomms8149, 7149-7149.
[19] N. Mondal, A. Samanta, Complete ultrafast charge carrier dynamics in photo–excited all–inorganic perovskite nanocrystals ($CsPbX_3$), Nanoscale 9 (2017) 1878–1885, https://doi.org/10.1039/C6NR09422H.
[20] X. Zhang, X. Bing, J. Zhang, G. Yuan, W.S. Xiao, All-inorganic perovskite nanocrystals for high-efficiency light emitting diodes: dual-phase $CsPbBr_3$-$CsPb_2Br_5$ composites, Adv. Funct. Mater. 26 (2016) 1600958, https://doi.org/10.1002/adfm.201600958.
[21] S. Seth, N. Mondal, S. Patra, A. Samanta, Fluorescence blinking and photoactivation of all-inorganic perovskite nanocrystals, $CsPbBr_3$ and $CsPbBr_2I$, J. Phys. Chem. Lett. 7 (2016) 266–271, https://doi.org/10.1021/acs.jpclett.5b02639.
[22] M. Gaponenko, A. Lutich, N. Tolstik, A. Onushchenko, A. Malyarevich, E. Petrov, K. Yumashev, Observation of linear-polarization-sensitivity in the microwave-radiation-induced magnetoresistance oscillations, Phys. Rev. B 82 (2010) 125320, https://doi.org/10.1063/1.4848372.
[23] P. Jing, J. Zheng, M. Ikezawa, X. Liu, S. Lv, X. Kong, J. Zhao, Y. Masumoto, Temperature-dependent photoluminescence of CdSe-core CdS/CdZnS/ZnS-multishell quantum dots, J. Phys. Chem. C 113 (2009) 13545–13550, https://doi.org/10.1021/jp902080p.

[24] Y. Zhao, C. Riemersma, F. Pietra, R. Koole, C.D.M. Donegá, A. Meijerink, High-temperature luminescence quenching of colloidal quantum dots, ACS Nano 6 (2014) 9058–9067, https://doi.org/10.1021/nn303217q.
[25] V. Babin, P. Fabeni, M. Nikl, G. Pazzi, I. Sildos, N. Zazubovich, S. Zazubovich, Polarized luminescence of $CsPbBr_3$ nanocrystals (quantum dots) in CsBr:Pb single crystal, Chem. Phys. Lett. 314 (1999) 31–36, https://doi.org/10.1016/S0009-2614(99)01110-0.
[26] M. Nikl, K. Nitsch, E. Mihokova, K. Polak, P. Fabeni, G.P. Pazzi, M. Gurioli, R. Phani, S. Santucci, A. Scacco, Optical properties of $Pb^{2+}$-based aggregated phases in CsBr Thin film and single crystal matrices, Radiat. Eff. 150 (1999) 341–345, https://doi.org/10.1080/10420159908226254.
[27] A. Voloshinovskii, S. Myagkota, A. Gloskovskii, S. Zazubovich, Luminescence of $CsPbCl_3$ microcrystals in CsCl:Pb and $PbCl_2$:Cs crystals under synchrotron excitation, Phys. Solid State 43 (2001) 1885–1891, https://doi.org/10.1134/1.141062.
[28] A. Balena, A. Perulli, M. Fernandez, M.L. Giorgi, G. Nedelcu, M. Kovalenko, M. Anni, Temperature dependence of the amplified spontaneous emission from $CsPbBr_3$ nanocrystal thin films, J. Phys. Chem. C 122 (2018) 5813–5819, https://doi.org/10.1021/acs.jpcc.8b01419.
[29] C. Wolf, T.-W. Lee, Exciton and lattice dynamics in low-temperature processable $CsPbBr_3$ thin-films, Mater. Today Energy 7 (2018) 199–207, https://doi.org/10.1016/j.mtener.2017.09.010.
[30] Z. Shi, S. Li, Y. Li, H. Ji, X. Li, D. Wu, T. Xu, Y. Chen, Y. Tian, Y. Zhang, Strategy of solution-processed all-inorganic heterostructure for humidity/temperature-stable perovskite quantum dot light-emitting diodes, ACS Nano 12 (2018) 1462–1472, https://doi.org/10.1021/acsnano.7b07856.
[31] Q.A. Akkerman, V. D'Innocenzo, S. Accornero, A. Scarpellini, A. Petrozza, M. Prato, L. Manna, Tuning the optical properties of cesium lead halide perovskite nanocrystals by anion exchange reactions, J. Am. Chem. Soc. 137 (2015) 10276–10281, https://doi.org/10.1021/jacs.5b05602.
[32] L. Protesescu, S. Yakunin, M.I. Bodnarchuk, F. Krieg, R. Caputo, C.H. Hendon, R.X. Yang, A. Walsh, M.V. Kovalenko, Nanocrystals of cesium lead halide perovskites ($CsPbX_3$, X = Cl, Br, and I): novel optoelectronic materials showing bright emission with wide color gamut, Nano Lett. 15 (2015) 3692–3696, https://doi.org/10.1021/nl5048779.
[33] D.K. Sharma, S. Hirata, V. Biju, M. Vacha, Stark effect and environment-induced modulation of emission in single halide perovskite nanocrystals, ACS Nano 13 (2019) 624–632, https://doi.org/10.1021/acsnano.8b07677.
[34] S. Singh, C. Li, F. Panzer, K. Narasimhan, A. Graeser, T.P. Gujar, A. Köhler, M. Thelakkat, S. Huettner, D. Kabra, Effect of thermal and structural disorder on the electronic structure of hybrid perovskite semiconductor $CH_3NH_3PbI_3$, J. Phys. Chem. Lett. 7 (2016) 3014–3021, https://doi.org/10.1021/acs.jpclett.6b01207.
[35] M. Jones, S.S. Lo, G.D. Scholes, Signatures of exciton dynamics and carrier trapping in the time-resolved photoluminescence of colloidal CdSe nanocrystals, J. Phys. Chem. C 113 (2009) 18632–18642, https://doi.org/10.1021/jp9078772.
[36] L. Yang, W. Zhai, P. Gu, T. Zhang, W. Peng, W. Liu, C. Tian, Y. Wang, Z. Yu, The exciton and phonon coupling in temperature-dependent photoluminescence of colloidal PbSe nanocrystals, Optik-Inter. J. Light and Electron Optics 124 (2013) 3059–3062, https://doi.org/10.1016/j.ijleo.2012.09.032.
[37] J. Chen, S. Wang, Y. Du, L. Chen, Temperature-dependent Photoluminescence Study of $Pb^{2+}$ Doped Strontium Iodide, IEEE NSS/MIC, 2013, p. 6829659, https://doi.org/10.1109/NSSMIC.2013.6829659.
[38] J. Li, X. Yuan, P. Jing, J. Li, M. Wei, J. Hua, J. Zhao, L. Tian, Temperature–dependent photoluminescence of inorganic perovskite nanocrystal films, RSC Adv. 6 (2016) 78311–78316, https://doi.org/10.1039/C6RA17008K.
[39] K. Wei, R. Chen, T. Jiang, X. Cheng, X. Zheng, Z. Xu, Temperature-dependent excitonic photoluminescence excited by two-photon absorption in perovskite $CsPbBr_3$ quantum dots, Opt. Lett. 41 (2016) 3821–3824, https://doi.org/10.1364/OL.41.003821.
[40] C. Yu, C. Zhuo, J.J. Wang, W. Pfenninger, N. Vockic, J.T. Kenney, S. Kai, Temperature dependence of the band gap of perovskite semiconductor compound $CsSnI_3$, J. Appl. Phys. 110 (2011): 063526, https://doi.org/10.1063/1.3638699.
[41] J. Lin, L. Gomez, W.C. De, Y. Fujiwara, T. Gregorkiewicz, K. Suenaga, Direct observation of band structure modifications in nanocrystals of $CsPbBr_3$ perovskite, Nano Lett. 16 (2016) 7198–7202, https://doi.org/10.1021/acs.nanolett.6b03552.
[42] S. Poltavtsev, B. Stroganov, Experimental investigation of the oscillator strength of the exciton transition in GaAs single quantum wells, Phys. Solid State 52 (2010) 1899–1905, https://doi.org/10.1134/S1063783410090180.
[43] J. Krustok, H. Collan, K. Hjelt, Does the low-temperature Arrhenius plot of the photoluminescence intensity in CdTe point towards an erroneous activation energy? J. Appl. Phys. 81 (1997) 1442–1445, https://doi.org/10.1063/1.363903.
[44] H. He, Q. Yu, L. Hui, L. Jing, J. Si, Y. Jin, N. Wang, J. Wang, J. He, X. Wang, Exciton localization in solution-processed organolead trihalide perovskites, Nat. Commun. 7 (2016) 10896, https://doi.org/10.1038/ncomms10896.
[45] M. Hauser, A. Hepting, R. Hauschild, H. Zhou, J. Fallert, H. Kalt, C. Klingshirn, Absolute external luminescence quantum efficiency of zinc oxide, Appl. Phys. Lett. 92 (2008) 211105, https://doi.org/10.1063/1.2937442.
[46] L. Jethi, T. Mack, M. Krause, S. Drake, P. Kambhampati, The effect of exciton-delocalizing thiols on intrinsic dual emitting semiconductor nanocrystals, ChemPhysChem 17 (2016) 665–669, https://doi.org/10.1002/cphc.201501049.
[47] M. Reshchikov, Temperature dependence of defect-related photoluminescence in III-V and II-VI semiconductors, J. Appl. Phys. 115 (2014): 012010, https://doi.org/10.1063/1.4838038.
[48] H. Shibata, Negative thermal quenching curves in photoluminescence of solids, Jpn. J. Appl. Phys. 37 (1998) 550–553, https://doi.org/10.1143/JJAP.37.550.
[49] J. Li, L. Luo, H. Huang, C. Ma, Z. Ye, J. Zeng, H. He, 2D behaviors of excitons in cesium lead halide perovskite nanoplatelets, J. Phys. Chem. Lett. 8 (2017) 1161–1168, https://doi.org/10.1021/acs.jpclett.7b00017.
[50] H. Shunsuke, H. Jimpei, I. Masashi, G. Kazuo, Structural phase transitions in $CsPbBr_3$, J. Phys. Soc. Japan 37 (1974) 1393–1398, https://doi.org/10.1143/JPSJ.37.1393.
[51] Y. Sun, L. Wang, Y. Liu, Y. Ren, Birnessite-type $MnO_2$ nanosheets with layered structures under high pressure: elimination of crystalline stacking faults and oriented laminar assembly, Small 11 (2015) 300–305, https://doi.org/10.1002/smll.201400892.
[52] M. Donega, M. Bode, A. Meijerink, Size- and temperature-dependence of exciton lifetimes in CdSe quantum dots, Phys. Rev. B Condens. Matter Phys. 74 (2006): 085320, https://doi.org/10.1103/PhysRevB.74.085320.
[53] S. Crooker, J. Hollingsworth, S. Tretiak, V. Klimov, Spectrally resolved dynamics of energy transfer in quantum-dot assemblies: towards engineered energy flows in artificial materials, Phys. Rev. Lett. 89 (2002) 186802, https://doi.org/10.1103/PhysRevLett.89.186802.
[54] M. Jones, S. Lo, G. Scholes, Quantitative modeling of the role of surface traps in CdSe/CdS/ZnS nanocrystal photoluminescence decay dynamics, Proc. Natl. Acad. Sci. U.S.A. 106 (2009) 3011–3016, https://doi.org/10.1073/pnas.0809316106.